

# Fate of Lu(III) sorbed on 2-line ferrihydrite at pH 5.7 and aged for 12 years at room temperature. I: insights from ICP-OES, XRD, ESEM, AsFIFFF/ICP-MS, and EXAFS spectroscopy

Nicolas Finck<sup>1</sup> · Muriel Bouby<sup>1</sup> · Kathy Dardenne<sup>1</sup>

## Abstract

Two-line ferrihydrite (2LFh) was aged for 12 years under ambient conditions and sheltered from light in the presence of Lu(III) used as surrogate for trivalent actinides. 2LFh aging produced hematite rhombohedra with overgrown acicular goethite particles. Analysis of the homogeneous suspension by asymmetrical flow field-flow fractionation (AsFIFFF) coupled to ICP-MS indicated that particles have a mean hydrodynamic diameter of about 140 nm and the strong correlation of the Fe and Lu fractograms hinted at a structural association of the lanthanide with the solid phase(s). Unfortunately, recoveries were low and thus results cannot be considered representative of the whole sample. The suspension was centrifuged and X-ray absorption spectroscopy (XAS) at the Lu  $L_3$ -edge on the settled particles indicated that Lu(III) is sixfold coordinated by oxygen atoms, pointing to a retention by structural incorporation within particles. This result is consistent with AsFIFFF results on the same suspension without centrifugation. The detection of next nearest Fe and O atoms were consistent with the structure of goethite, ruling out incorporation within hematite. After centrifugation of the suspension, only nanoparticulate needle-like particles, very likely goethite, could be detected in the supernatant by ESEM. AsFIFFF data of the supernatant were comparable to that obtained for the homogeneous suspension, whereas XAS indicated that Lu(III) is predominantly present as dissolved species in the supernatant. Results from both techniques can be interpreted as a major fraction of Lu present as aqueous ions and a minor fraction as structurally incorporated. Findings from this study are corroborated by STEM-HAADF data and results from DFT calculations in a companion paper.

**Keywords** Ferrihydrite transformation · Hematite · Goethite · Lutetium · Flow field-flow fractionation · ICP-MS · X-ray absorption spectroscopy

## Introduction

Iron (hydr)oxides are common compounds that are widespread in nature (Cornell and Schwertmann 1996). For

example, the hydrous ferric oxyhydroxide ferrihydrite (Fh) occurs in Fe-bearing waters (Carlson and Schwertmann 1981), soils and sediments (Jambor and Dutrizac 1998) and forms upon corrosion of iron and steel. However, Fh is thermodynamically unstable and with time transforms into more stable oxides such as hematite and/or goethite. Hematite is formed by an internal dehydration/rearrangement process within Fh particles, whereas the goethite formation proceeds via Fh dissolution followed by nucleation and growth (Schwertmann and Cornell 1991). Depending on the chemical conditions, hematite, goethite, or a mixture of the two can form.

Because of their ubiquity in soils and sediments and their high reactivity in respect to sorption reactions, iron (hydr)oxides are important regulators of the concentration and distribution of pollutants. Freshly precipitated Fh consists

✉ Nicolas Finck  
nicolas.finck@kit.edu

✉ Muriel Bouby  
muriel.bouby@kit.edu

Kathy Dardenne  
kathy.dardenne@kit.edu

<sup>1</sup> Institute for Nuclear Waste Disposal (INE), Karlsruhe Institute of Technology (KIT), P.O. Box 3640, 76021 Karlsruhe, Germany

of very small particles and thus has a high reactive surface area. Consequently, small amounts of ferrihydrite nanoparticles (NPs) may dominate the ion-binding properties of soils and sediments where they are present (Hiemstra and Van Riemsdijk 2009). Because of their small size, NPs may also be relatively mobile and thus influence the migration behavior of heavy metal ions and radionuclides from polluted sites or nuclear waste repositories in natural aquifer systems (Lion et al. 1982; Lu et al. 1998; Novikov et al. 2006; Schäfer et al. 2003).

Ferrihydrite and its transformation products hematite and goethite have been extensively used in pollutant uptake studies (e.g., Cornell and Schwertmann 1996 and references therein). Most studies focused on the retention by contacting, e.g., cations with pre-existing iron (hydr)oxides; however, most effective immobilization may be achieved by incorporation within the bulk solid. Yet, studies on the retention of (heavy) metal ions by incorporation within the bulk structure of hematite and goethite have been reported and aimed at mimicking mechanisms likely to occur in contaminated surface or subsurface environments. In these experiments, Fe (hydr)oxides were formed by aging either pre-formed Fh contacting the pollutant or more frequently Fh that was synthesized in the presence of pollutants (e.g., Ni (Cornell et al. 1992), Cd (Sun et al. 1996), Pb (Ford et al. 1997)). Most studies were performed at elevated temperatures (up to 70 °C) for periods up to 1 month; the presence of such pollutants retarded the Fh transformation and the extend of substitution for Fe(III) depended on the ionic size.

Actinides are long-lived and radiotoxic radionuclides (RN) present in high-level nuclear waste (HLW) and iron (hydr)oxides are expected to form upon corrosion of steel canisters in aqueous environments. These neoformed iron phases can represent an additional effective chemical barrier hindering the migration of actinides to the repository far field. Several studies on the possible structural incorporation of actinides within iron oxides have been reported. Aging at elevated temperature a Fh suspension spiked with either U(VI) or Np(V) results in the substitution of the actinide for Fe(III) within the bulk structure of hematite (Bots et al. 2016; Marshall et al. 2014). Reported XAS data also suggested that aging Fh at 25 °C in the presence of Am(III) results in trivalent actinide substitution for Fe(III) within a goethite-like structure (Stumpf et al. 2006), and more recently that Am(III) can be accommodated within magnetite in co-precipitation experiments (Finck et al. 2016).

Several studies also focused on deciphering the actual binding mode of trivalent actinides by iron oxides using their non-radioactive chemical surrogates, the trivalent lanthanides (Ln(III)). For example, aging pre-formed Fh in the presence of Lu(III) at 70 °C and at circumneutral pH values resulted in the formation of a mixture of hematite and goethite and X-ray absorption spectroscopy indicated a preferential Lu(III)

incorporation within the structure of hematite rather than into goethite (Dardenne et al. 2002; Bouby et al. 2004). Similarly, the conversion in alkaline medium and at elevated temperature (70 °C) of Fh prepared in the presence of Nd(III) resulted in the formation of Nd-containing hematite and Nd-free goethite (Nagano et al. 1999). In this latter study, structural similarities between  $\alpha$ -Fe<sub>2</sub>O<sub>3</sub> and Nd<sub>2</sub>O<sub>3</sub> were believed to be essential. The incorporation of Eu(III) within hematite by co-precipitation at elevated temperature has also been reported (Freyria et al. 2013). In this study, XRD and TEM data indicated a replacement of Fe(III) by Eu(III) with an enrichment of the lanthanide at the core. Interestingly, in these studies performed at elevated temperature, ferrihydrite converted into a mixture of hematite and goethite but the lanthanide preferentially substituted for Fe(III) within hematite.

In the far field of deep HLW repositories and in surface and subsurface environments, temperatures are expected to be lower than in a repository near-field, thereby possibly modifying the mechanism of Fh transformation and thus affecting the geochemical behavior of pollutants such as RN. Elevated temperatures favor Fh dehydration and particle aggregation and thereby promote hematite formation (Cornell and Schwertmann 1996; Cudennec and Lecerf 2006). At lower temperatures more representative of ambient conditions, the transformation may be kinetically slower and affect the nature and/or the proportion of the transformation products. Similarly, increased contact time in aqueous environments can also modify the binding environment of pollutants retained by mineral phases upon phase transformation or recrystallization (e.g., (Finck et al. 2016)). Consequently, longer time spans are required to obtain important information on the long-term geochemical behavior of trivalent actinides when associated with iron (hydr)oxides.

In this study, pre-formed Fh was contacted with Lu(III), used as homolog for trivalent actinides, and aged for 12 years under ambient conditions. The morphology and mineralogical composition of the transformation products, and the Lu(III) repartition between the solid and the liquid phase were determined. Information on the Lu(III) association mode with the particles was obtained by application of the asymmetrical flow field-flow fractionation (AsFFFF) technique coupled to sensitive detection techniques using similar methodology as in earlier works with various NPs (e.g., (Bouby et al. 2011; Bouby et al. 2012; Bouby et al. 2015; Huber et al. 2012)) whereby Fe was used as fingerprint of the presence of Fe phases (hematite and/or goethite). Information on the retention mode and on the nature of the host phase was obtained by X-ray absorption spectroscopy at the Lu *L*<sub>3</sub>-edge. Complementary STEM-HAADF investigations on the same sample and DFT calculations will be presented in an companion paper (Yokosawa et al. 2018).

## Materials and methods

### Sample preparation

The sample was prepared with ultrapure water (18.2 M $\Omega$  cm, Milli-Q Plus system (Millipore)) and reagents of ACS grade or higher. Two-line ferrihydrite was prepared as described in (Schwertmann and Cornell 1991). Briefly, 10 g Fe(NO<sub>3</sub>)<sub>3</sub>·9H<sub>2</sub>O were dissolved in 125 mL ultrapure water and 82.5 mL 1 M KOH were added under stirring. The resulting suspension was washed with water by centrifuging eight times. Subsequently, Lu(III) ([Lu(III)]<sub>tot</sub> = 1.6 × 10<sup>-4</sup> mol/L) was added to this suspension (2.7 g/L) under stirring and the pH adjusted to 5.88 ± 0.05 (thereafter, the notation 5.88(5) is used to indicate the uncertainty). This sample was then left to age for 12 years under ambient conditions in a closed bottle in the dark before recording X-ray absorption spectra. For practical reasons, the analysis by AsFIFFF was performed 3 years after XAS measurements, i.e., on a 15 years old sample. After aging, the pH of the homogeneous suspension was 5.67(5).

For analysis, the suspension was stirred before sampling and where indicated an aliquot was centrifuged for 35 min at 4000 rpm (Heraeus Megafuge 2.0R). These conditions were chosen to separate the smallest particles in suspension because in deep disposal sites these particles are more likely to be transported by groundwater over long distances, investigations on Lu(III) retention by these particles are thus of high importance. Thereafter, the homogeneous suspension is named sample T2, the supernatant after centrifugation is named sample T2 super and the settled solid is named sample T2 solid. For each sample, various complementary analytical techniques were applied (Table 1). Information on the elemental composition was provided by acidic digestion followed by quantification of the solution by ICP-OES (Perkin Elmer Elan 2000 DV) or ICP-MS (X-Series2, Thermo Scientific, Germany). Information on the size and shape of the particles was provided by electron microscopy using an environmental scanning electron microscope (ESEM, Quanta 650 FEG (FEI)) and an AsFIFFF hyphenated equipment (see below). The mineralogical composition of T2 solid was determined by X-ray diffraction (XRD) using a D8 Advance (Bruker) diffractometer (Cu K $\alpha$  radiation) equipped with an energy-dispersive detector (Sol-X). Phases were identified by comparison with the PDF-2 database using the EVA 3.1 software (Bruker) and fits to the data were provided by the TOPAS 4.2 software (Bruker) using the reported structures of hematite (Maslen et al. 1994) and goethite (Hazemann et al. 1991).

### Asymmetrical flow field-flow fractionation coupled to UV-visible, LLS, and ICP-MS detections

The general and detailed principles and description of the field-flow fractionation methods can be found elsewhere

(Giddings 1993; Giddings et al. 1976; Schimpf et al. 2000; Wahlund and Giddings 1987). Size fractionation is achieved in a thin ribbon-like channel in a laminar carrier flow, while applying a crossflow perpendicularly to the channel flow. The elution sequence of colloidal species is determined by their diffusion coefficient and thus by their size. A complete description of the used AsFIFFF system (HRFFF 10.000 AF4, Postnova Analytics) can be found in (Bouby et al. 2008). The accumulation wall of the channel is a semipermeable ultrafiltration membrane made of regenerated cellulose of 5 kDa pore size (Postnova Analytics). A PTFE spacer of 0.5 mm in height delimits the channel thickness. The used carrier is a 10<sup>-2</sup> mol/L MES buffer (2-(*N*-morpholino)ethanesulfonic acid) solution of pH 5.70(5), matching within uncertainties the pH of the sample, and this solution was degassed prior to use by a vacuum degasser. The channel flow rate is maintained at 0.7 mL/min during the fractionation of the suspensions. The initial crossflow represents 75% of the inflow and decreased linearly by 5% every 60 s. After 900 s, no more crossflow is applied and the elution goes on during additional 900 s. These fractionation conditions have been tested carefully, details can be found in (Bouby et al. *In Preparation*).

The suspension (i.e., sample T2 or T2 super) is vigorously shaken prior to dilution in the eluent (MES buffer) and injected without any filtration (injected sample volume: 100  $\mu$ L). The sample is injected during 2 min and then focused during two additional minutes before the start of the elution. The injected concentrations are low enough to avoid any overloading of the channel due to charge repulsion effects between charged particles (Schimpf et al. 2000; Ngo Manh et al. 2001; Wijnhoven et al. 1996). The reproducibility of peak positions even at lowest concentrations is excellent, even by using this carrier of moderate ionic strength. In this study, Fe- and Lu-ICP-MS fractograms for each sample were obtained by diluting 10 times the suspensions in the eluent just before injection, and two successive measurements are plotted to demonstrate the good reproducibility.

From the channel, the effluent is directed to a UV-visible detector (Waters, USA) for recording the absorption signal at 225 nm. From the UV-visible detector, the effluent goes through a laser light scattering (LLS) detector which is a commercial DAWN-DSP-F light scattering photometer (Wyatt Technology Corp., Santa Barbara, USA) running with the Astra software (v3.0). A 5 mW HeNe laser provides the incident light beam ( $\lambda_{em}$  = 632 nm) and is directed through the detector cell of 70  $\mu$ L volume. Scattered light is detected by an array of 18 photodiodes arranged at different angles relative to the incoming laser beam. Information on colloid size is obtained after calibration of the arrangement with a mixture of polystyrene colloids. Stock solutions of reference carboxylated polystyrene particles of different sizes (24, 40, 60, 97, 217, 420, and 495 nm (Magsphere, Pasadena, USA)) were prepared in ultrapure water with an aliquot of NaOH (final

**Table 1** Results obtained for the investigated samples by application of various analytical techniques

Technique	Sample T2	Sample T2_solid	Sample T2_super
ICP OES ( $\pm 5\%$ )	[Fe] <sub>tot, ini</sub> = $3.1 \times 10^{-2}$ mol/L [Lu] <sub>tot, ini</sub> = $1.6 \times 10^{-4}$ mol/L  Fe/Lu = $55 \pm 5$ (mass ratio) $180 \pm 5$ (mol ratio)	/	[Fe] <sub>tot</sub> = $2.5 \times 10^{-3}$ mol/L (= 8% [Fe] <sub>tot, ini</sub> ) [Lu] <sub>tot</sub> = $9.1 \times 10^{-5}$ mol/L (= 57% [Lu] <sub>tot, ini</sub> )  Fe/Lu = $9 \pm 1$ (mass ratio) $28 \pm 5$ (mol ratio)
SEM	Rhomboheda (hematite) with overgrown needles (goethite): 100 200 nm	/	Needles (goethite): < 500 nm length 10 30 nm diameter
XRD	/	~70% hematite ~30% goethite	/
AsFIFFF + UV vis./LLS/ICP MS	Hydrodynamic size distribution Mode: $138 \pm 7$ nm  Fe/Lu ratio $196 \pm 17$ (mass) $616 \pm 53$ (mol)  Recoveries (%)    Fe: $18.9 \pm 6.1$ Lu: $4.4 \pm 1.4$	/	Hydrodynamic size distribution Mode: $135 \pm 9$ nm  Fe/Lu ratio $215 \pm 59$ (mass) $675 \pm 184$ (mol)  Recoveries (%)    Fe: $11.8 \pm 2.7$ Lu: $0.2 \pm 0.06$
EXAFS	/	Lu very likely substitutes for Fe within goethite	Lu predominantly present as dissolved species

pH 9.3). Stock solutions of polystyrene sulfonate standards (PSS) were prepared in a similar way from the salts (Polyscience, Germany). The corresponding molecular weights employed were 0.891, 1.67, 3.42, 6.43, 15.8, and 33.5 kDa. Different mixtures for calibration were obtained by appropriate dilution of these stock solutions in the eluent used for the fractionation system ( $10^{-2}$  mol/L MES buffer at pH 5.70(5)). Finally, for the analysis of the elemental composition of the colloids, the effluent is mixed with 6% nitric acid containing 10  $\mu$ g/L Rh as an internal standard and introduced into the ICP-MS (X-Series2, Thermo Scientific, Germany) at a constant rate of 0.5 mL/min. Recoveries were determined by injecting the acidified sample directly (i.e., without passing through the fractionation channel) and by comparing the recorded area. For details concerning the determination of the recoveries and the quantification, see (Bouby et al. 2008).

### X-ray absorption spectroscopy (XAS)

Lu  $L_{3-}$ edge X-ray absorption spectra were collected at the INE-Beamline for actinide science (Rothe et al. 2012) at the synchrotron light source ANKA (Karlsruhe, Germany) with a storage ring energy of 2.5 GeV and a ring current of 90–160 mA. The double crystal monochromator was equipped with a pair of Si(111) crystals. Energy calibration was done by assigning the first inflection point of the  $K$ -edge X-ray absorption near edge structure (XANES) recorded from a Zn foil to 9659 eV, and this reference was measured in parallel with all samples. Data were collected either in transmission or in fluorescence detection mode by using a silicon drift detector (Vortex, SII, NanoTechnology).  $\text{Lu}_2\text{O}_3$  and  $\text{Lu(III)}_{\text{aq}}$  ions

( $\text{Lu}_2\text{O}_3$  dissolved in 2%  $\text{HClO}_4$ ,  $[\text{Lu(III)}]_{\text{tot}} = 0.08$  M) were also measured and used as reference compounds.

Data analysis was performed by using Athena and Artemis interfaces to the Ifeffit software (Ravel and Newville 2005). Extended X-ray absorption fine structure (EXAFS) spectra ( $\chi(k)$ ) were extracted from the raw data and Fourier transforms (FTs) were obtained from the  $k^3 \times \chi(k)$  functions. The data were fit in  $R$ -space by using a combination of single scattering paths. For each coordination shell, phase and amplitude functions were calculated separately with feff8.4 (Ankudinov et al. 1998), and the amplitude reduction factor was set to 1.0. Uncertainties on distances and coordination numbers are indicated in parentheses in Table 2. The fit quality was quantified by the  $R_f$ -factor representing the absolute misfit between theory and experimental data. XAS is an element specific technique, meaning that the recorded signal corresponds to the sum of contributions from all species. However, for samples containing more than one species this technique may not be able to clearly identify the presence of species present in minor amounts (e.g., few percent).

## Results and discussion

### Morphology, mineralogical and elemental compositions

Scanning electron micrographs (Fig. 1) indicate that sample T2 consists of a mixture of rhombohedra and needles, whereas T2 super consists only of needles. Considering typical crystal habits, rhombohedra may correspond to hematite and needles

**Table 2** Quantitative EXAFS analysis of the samples and reference compounds

Sample	FT range <sup>a</sup> [ $\text{\AA}^{-1}$ ]	Fit range <sup>b</sup> [ $\text{\AA}$ ]	Path				$\Delta E_0$ [eV]	$R_f (\times 10^3)$
			Shell	$N$	$R$ [ $\text{\AA}$ ]	$\sigma^2$ [ $\text{\AA}^2$ ]		
Lu(III) <sub>aq</sub>	3.2 14.0	1.6 2.4	O1	8.0	2.31(2)	0.007	4.1(4)	1.3
Lu <sub>2</sub> O <sub>3</sub>	3.5 15.3	1.6 3.7	O1	6.0	2.22(2)	0.006	6.1(7)	8.3
			Lu1	6.0	3.44(2)	0.005		
			Lu2	6.0	3.93(4)	0.007		
T2 <sub>super</sub>	3.3 9.3	1.5 2.4	O1	8.0(4)	2.31(2)	0.006	4.3(11)	4.0
T2 <sub>solid</sub>	3.3 9.0	1.4 4.1	O1	5.9(3)	2.20(2)	0.009	4.5(11)	3.7
			Fe1	1.8(4)	3.07(3)	0.008		
			O2	2.6(5)	3.28(7)	0.006		
			Fe2	2.4(7)	3.49(4)	0.007		

The number in parentheses indicates the uncertainty on coordination numbers and interatomic distances; otherwise, the parameter was held fixed.  $R$  interatomic distance,  $N$  coordination number,  $\sigma^2$  mean square displacement,  $\Delta E_0$  energy shift,  $R_f$  figure of merit of the fit.

<sup>a</sup> Fourier transformed range

<sup>b</sup>  $R + \Delta R$  interval for the fit

to goethite (Cornell and Schwertmann 1996). No other phase can be seen in any sample, indicating that Fh quantitatively transformed. Electron micrographs further indicate that hematite is not present as a separate phase but structurally associated with goethite, as acicular goethite outgrowths on hematite centers. This association mode was already reported in literature (Boudeulle and Muller 1988; Cornell 1985). Structures of both goethite and hematite are based on an hexagonal close-packed anion array and some of the interplanar spacings of the two compounds are similar, thus facilitating epitaxial growth (Cornell and Schwertmann 1996). In sample T2, particles

have sizes of about 100–200 nm and in T2<sub>super</sub> needles have about 10–30 nm in diameter and < 500 nm in length. These values are consistent with those obtained by transmission electron microscopy (Yokosawa et al. 2018).

The presence of goethite and hematite in sample T2 indicated by SEM was corroborated by XRD analysis. Furthermore, powder X-ray diffractogram modeling provided quantitative information: sample T2<sub>solid</sub> consists of ~70% hematite and ~30% goethite (Fig. 1). The content of Fe phases in the supernatant was too low for XRD analysis but based on typical crystal habit only goethite may be present.

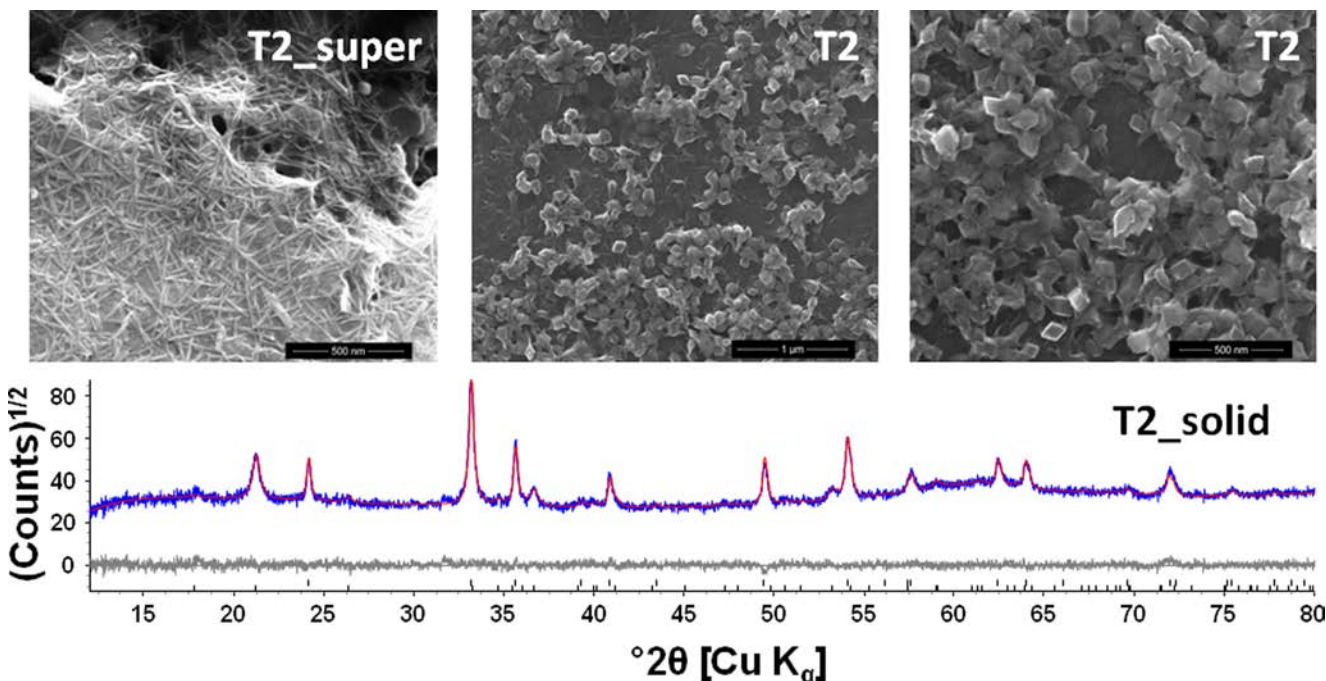


**Fig. 1** Scanning electron micrographs of samples T2<sub>super</sub> and T2 (upper part) and experimental and modeled X ray diffractogram of sample T2<sub>solid</sub> where the blue line represents the experimental data, the red line the fit to the experimental data, and the gray line the residual (lower part)

Sample T2 contains  $3.1 \times 10^{-2}$  mol/L total Fe and  $1.6 \times 10^{-4}$  mol/L total Lu (Table 1). Centrifuging sample T2 removed particles representing 92% of total Fe, and thus 8% of total Fe is present either as dissolved Fe species or more likely as suspended nanoparticulate iron phases because of the low solubility of  $\text{Fe(III)}_{\text{aq}}$  under these chemical conditions. Chemical analysis further indicated that the Lu(III) concentration in T2 super is reduced by about 50% compared to that of the original suspension, indicating that half of total Lu(III) is associated with the solid transformation products in T2 solid and thus that the other half is present in the supernatant either as dissolved species or associated with nanoparticulate iron phases. Consequently, the Fe/Lu mass ratio (Table 1) in sample T2 super ( $9 \pm 1$ ) is lower than in sample T2 ( $57 \pm 5$ ), whereas this ratio is highest in sample T2 solid ( $181 \pm 6$ ).

### AsFIFFF combined with UV-visible, LLS and ICP-MS detections

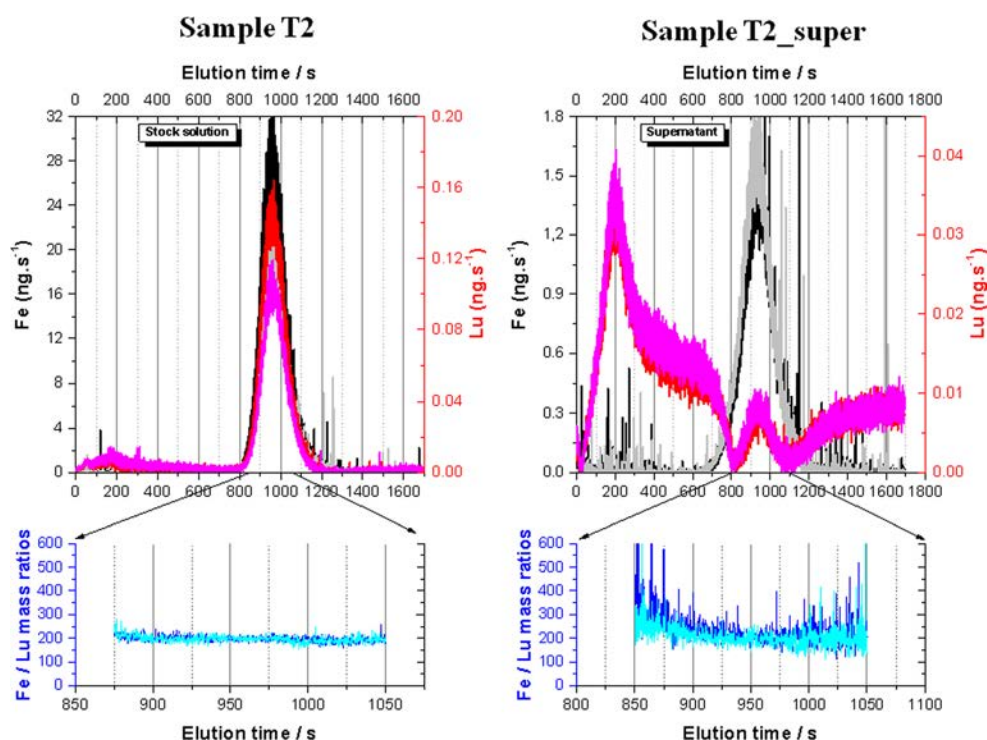
The Fe- and Lu-ICP-MS fractograms obtained for the stock suspension (sample T2, Fig. 2) are slightly asymmetric and the reproducibility is very good. At the rather high colloid concentrations injected, the UV-visible detection ( $\lambda = 225$  nm) is easy while the LLS signal (detected at  $90^\circ$ ) is saturated during the measurement of the diluted stock solution. Nevertheless, the UV-visible and LLS detection (data not shown) confirm the position of the colloids indicated by the Fe-ICP-MS signals.

For sample T2, the Fe signal dominates with a peak maximum recorded at 952 s (elution time) and  $\sim 32$  ng (Fig. 2), and the Lu signal is perfectly correlated with that of Fe. This is compatible with a homogeneous adsorption or incorporation within the colloidal iron matrix. The shape of the Fe fractogram is quite narrow and comparable to fractograms obtained for the monomodal carboxylated polystyrene standard nanoparticles. Considering the AsFIFFF calibration made with these standards, the hydrodynamic size distribution of the detected colloidal iron nanoparticles is not expanded and comprised between 97 nm (peak maximum at  $910 \pm 2$  s) and 217 nm (peak maximum at  $1021 \pm 4$  s). This can be explicitly seen in Fig. 3. According to the calibration equation derived from the position of the peak maxima (elution time) of all used standards ( $\text{size} = f(\text{elution time})$ ), the measurements indicate that the size (i.e., hydrodynamic diameter) of the detected iron colloids (at  $952 \pm 8$  s) in the stock solution is  $138 \pm 7$  nm.

Fitting of the Fe-ICP-MS fractogram by a simple Gaussian centered at 964 s (using the Origin software, V.9.1) was attempted; however, it resulted in a poor modeling of the elution data in the range from 1050 to 1300 s due to the slight peak asymmetry. A better fit was obtained with two Gaussians centered at 954 s ( $\sim 140$  nm) and 1010 s ( $\sim 200$  nm), which might indicate the presence of (at least) two populations of iron colloids based on a size criteria.

Unfortunately, the sample recovery is very limited. This can be explained by a strong interaction with the membrane due to the membrane itself, to the applied fractionation

**Fig. 2** Upper panel: Fe (black and gray lines) and Lu ICP MS fractograms (red and pink lines) obtained after injection of sample T2 (left) or T2\_super (right) diluted by 10 in the eluent ( $10^{-2}$  mol/L MES) (dilutions were performed directly before injection). Lower panel: Fe/Lu mass ratio (blue lines). For each sample, two injections of 100  $\mu\text{L}$  each without filtration were performed and demonstrate the very good reproducibility



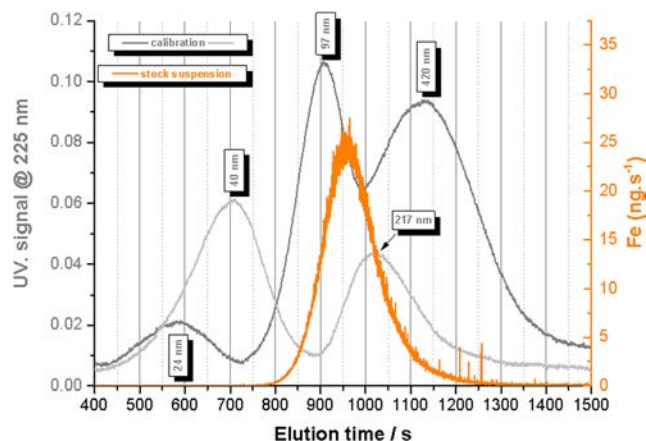


**Fig. 3** Comparison of fractograms obtained for the standard nanoparticles (calibration) and Fe colloids in sample T2 (sample diluted 10 times in eluent, mean of two measurements)

conditions, or to the formation of aggregates during the injection/focusing phases which will thus not be possible to elute and recover properly. This is clearly evidenced by a strong, increasing and persistent orange–reddish–brown coloration of the membrane. Only  $(18.9 \pm 6.1)$  % of the total iron and  $(4.4 \pm 1.4)$  % of total Lu present in the suspension are recovered, meaning that the main fraction of the injected sample is not eluted. Consequently, the obtained results are only a partial representation of the total sample. However, it can be concluded that a minimum of  $\sim 20\%$  of Fe is present in a colloidal form associated with  $\sim 4\%$  of the total Lu and that the major part of Lu is not associated with iron colloids. Nevertheless, the strong correlation of both fractograms hints at an homogeneous association of the eluted lutetium with iron colloids. A close inspection of the Fe/Lu mass ratio variation over a significant elution time range, i.e., colloidal fraction, strengthens this hypothesis: the obtained value is constant and equals  $196 \pm 17$  (Fe/Lu mole ratio of  $616 \pm 53$ ) (Fig. 2). Unfortunately, since both iron phases are structurally associated (goethite overgrown on hematite forming a single nanoparticle), it is not possible to identify more precisely with which iron phase(s) Lu is associated. Both iron phases cannot be fractionated and are consequently eluted simultaneously. At this stage, it thus can only be concluded that a minor but significant fraction of lutetium present is intimately associated with the detected iron colloids. Due to the irregular shape of the iron colloids (elongated needles on rhombohedra), results might better suggest a lutetium immobilization by incorporation within iron colloids rather than by surface adsorption which might have resulted in a less constant Fe/Lu ratio according to previous studies (Bouby et al. 2015; Finck et al. 2012). Information on the nature of the Lu species and on the phase(s) immobilizing Lu(III) will be obtained by probing the Lu  $L_3$ -edge by X-ray absorption spectroscopy (see below).

According to the elemental analysis (Table 1), the supernatant obtained by centrifuging sample T2 (i.e., sample T2 super)

still contains 8% of total Fe and 57% of total Lu. Information on Lu and residual iron particles in T2 super was obtained by recording Fe- and Lu-ICP-MS fractograms (Fig. 2). The results evidence the presence of iron colloids after the centrifugation step. The detection of Lu associated with residual iron colloids is heavily complicated by the presence of a large amount of dissolved Lu in suspension. Also, a “pure” lutetium peak (i.e., not correlated with an iron signal) is clearly detected at  $\sim 200$  s ( $\sim 4$  nm). This is visible as well on the Lu fractogram after injection of the stock suspension (sample T2). Nevertheless, the detection of lutetium associated with iron is still feasible but restricted to a narrower elution range.

The correlation between Fe and Lu is evident in the investigated range, and the Fe/Lu mass ratio is rather constant though noisier than for sample T2. The Fe/Lu mass ratio of  $215 \pm 59$  (mole ratio of  $675 \pm 184$ ) is within uncertainties comparable to that obtained for the stock suspension (sample T2,  $196 \pm 17$ ). The Fe peak maximum position (mode) occurs at  $(947 \pm 10)$  s, i.e., hydrodynamic size of  $135 \pm 9$  nm, a value similar to that obtained for sample T2 ( $138 \pm 7$  nm).

The recoveries for sample T2 super are lower than for the stock suspension: only  $(11.8 \pm 2.7)$  % of the total iron and  $(0.2 \pm 0.06)$  % of total Lu present in suspension are recovered in the colloidal fraction detected between 700 and 1300 s. The explanations given previously can explain this low recovery as well but for this sample SEM pictures (Fig. 1) reveal that the supernatant mainly contains needle-like iron nanoparticles which, according to the morphology, certainly consist of goethite. These needles have much less than 500 nm in length and around 10–20 nm in diameter. In a previous work, Sharma et al. (2009) demonstrated the use of centrifugation as an efficient method for separating colloidal gold nanorods from gold nanospheres. During centrifugation, nanoparticles move with different sedimentation velocities dictated by their Svedberg coefficients. Small differences in concentrations of nanoparticles, centrifugation parameters, and particle dimensions drove rods either to sediment out or to remain in suspension. The effectiveness of the sedimentation between rods and spheres depends on the ratio of equilibrium sedimentation velocities or their coefficients (Sharma et al. 2009). For single rods and single spheres, it appears that the central role in the separation is played by the ratio of the squares of their diameters rather than by the particle aspect ratio. Considering in this study a hydrodynamic diameter of  $\sim 138$  nm for rhombohedra and a diameter of 15 nm for needles in sample T2 super in a first approximation, the velocity ratio is greatly in favor of rhombohedra sedimentation (by a factor  $> 325$ ). This finding explains the composition of the supernatant after centrifugation as observed on the SEM picture, i.e., rhombohedra settled down whereas needles remained in suspension under the selected centrifugation parameters.

The elution of rod-like particles in the AsFIFFF was modeled by Phelan et al. (Phelan and Bauer 2007, 2009),

based on a particle diameter of 1 nm. They showed that rods continue to elute by a normal mode mechanism (increasing length based separation) up to a size of approximately 500 nm. For larger sizes, rods begin to elute much slower than predicted. This might be attributed to alignment of rods in the low velocity region along the accumulation wall (the membrane). Because iron particles in sample T2 super are needles of ~10–20 nm diameter, it is not possible to directly transpose the prediction from Phelan et al. to the present study; however, similar explanations might be proposed. The observed low recovery after injection of the supernatant, containing mainly needle-like iron nanoparticles, could be due to an attachment to the membrane, to the conditions selected for the elution (i.e. a rather high crossflow rate pushing the rods towards the accumulation wall, where aligned, they stay in lower velocity flow stream lines) or to a stacking of rods during the injection/focusing phase making them elute much slower or not at all.

Nevertheless, the mean hydrodynamic diameter deduced from AsFIFFF measurements on the recovered colloids agrees with the mean length size observed on SEM pictures. Despite the low recovery, the Lu detection is unequivocal and consistent with a homogeneous Lu immobilization onto/into goethite nanoparticles in the investigated size range. Actually, these “pure” goethite nanoparticles are not separated from the overgrown hematite-goethite particles upon injection of the stock suspension as (1) they seem to present the same hydrodynamic diameter and (2) they represent a maximum of less than 8% of the total iron injected in the stock solution. The recoveries are quite low (Table 1) which means that results are only representative of a minor part of the total sample.

## X-ray absorption spectroscopy

**X-ray absorption near edge structure** Lu(III)<sub>aq</sub> and Lu<sub>2</sub>O<sub>3</sub> were used as reference compounds for eightfold and sixfold coordinated Lu(III), respectively. Both compounds have comparable edge crest positions, but distinct positions of the maximum of the first oscillation after the edge crest (Fig. 4). This maximum is at ~4 eV lower energy in Lu(III)<sub>aq</sub> (9279.5(3) eV) than in Lu<sub>2</sub>O<sub>3</sub> (9283.4(3) eV) and can be attributed to differences in the distance from Lu to the first coordinating shell (Bianconi et al. 1983). For T2 super, the first oscillation after the edge crest is at a position similar to that of Lu(III)<sub>aq</sub>, whereas it is closer to that of Lu<sub>2</sub>O<sub>3</sub> in T2 solid. These results suggest that the first O shell is located at ~2.31 Å in T2 super and at ~2.22 Å in T2 solid, thus strongly pointing to differences in Lu binding environments.

**Extended X-ray absorption fine structure** The EXAFS spectrum of Lu(III)<sub>aq</sub> contains only a single wave frequency of decreasing amplitude indicating the presence of only one ordered shell. Accordingly, the Fourier transform (FT) contains only one peak that could be modeled with one O shell of

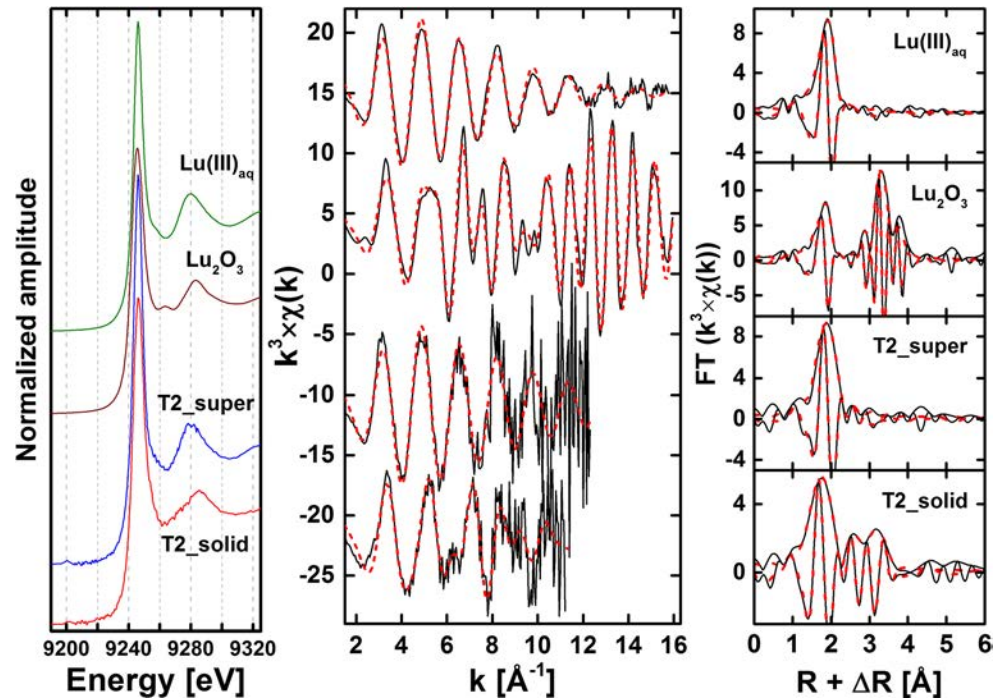
$N_{O1} = 8.0$  atoms at  $d(\text{Lu—O}) = 2.31(2)$  Å (Table 2), in good agreement with reported data (Persson et al. 2008). The spectrum of Lu<sub>2</sub>O<sub>3</sub> has distinct frequencies which are absent in that of Lu(III)<sub>aq</sub> and can be attributed to the presence of multiple ordered atomic shells. The FT contains several contributions that could be modeled considering O and Lu atoms with coordination numbers and interatomic distances in agreement with reported structural data (Qi et al. 2007).

Though noisier, the spectrum of T2 super is comparable to that of Lu(III)<sub>aq</sub> (Fig. 4), and the FT contains only one peak at  $R + \Delta R \sim 1.9$  Å that was modeled considering eight O atoms at  $d(\text{Lu—O1}) = 2.31(2)$  Å (Table 2), no higher distance O, Fe, and/or Lu atomic shell could be detected. This result hints at the presence of dissolved Lu(III) species in T2 super.

The spectrum of T2 solid differs in amplitude and frequency of the oscillations, and contains spectral features (e.g., at  $k \sim 6$  and  $\sim 9$  Å<sup>-1</sup>) that are absent in T2 super. The FT contains a first peak at  $R + \Delta R \sim 1.9$  Å, related to the presence of O atoms, and higher distance contributions at ~2.6 and ~3.3 Å. The data could be fitted considering a first O shell of about six atoms at  $d(\text{Lu—O1}) = 2.20(2)$  Å (Fig. 4, Table 2). Additional Fe and O shells at  $d(\text{Lu—Fe1}) = 3.07(3)$  Å and  $d(\text{Lu—Fe2}) = 3.49(4)$  Å, and at  $d(\text{Lu—O2}) = 3.28(7)$  Å, respectively, were used to model higher distance contributions. No neighboring Lu could be detected thus ruling out the presence of polymers. By comparison with the reported short range environment of Lu(III) forming surfaces complexes on various minerals including iron (hydr)oxides (Dardenne et al. 2001; Finck et al. 2009; Ohta et al. 2009), the sixfold Lu coordination by O atoms (O1 shell) is not compatible with the presence of such species in T2 solid. In contrast, it may be compatible with Lu located in an octahedral environment such as that available in both Fe phases (hematite and goethite) present in T2 solid.

The type of atomic shells surrounding successively Fe in hematite differs from that for Fe in goethite and can be used to identify the structure of the host phase. Hematite consists of FeO<sub>6</sub> octahedra which are connected by edge- and face-sharing, whereas goethite consists of double bands of edge-sharing FeO<sub>3</sub>(OH)<sub>3</sub> octahedra linked by corner-sharing in such a way as to form 2 × 1 octahedra “tunnels” crossed by hydrogen bridges (Schwertmann and Cornell 1991). In both structures, the Fe(III) first coordination sphere consists in O atoms but the arrangement of next nearest neighbors differs: it consists of only Fe shells at 2.89, 2.97, and 3.36 Å in hematite (Maslen et al. 1994) and of Fe shells at 3.02, 3.30, and 3.45 Å together with one O shell at 3.22 Å in goethite (Hazemann et al. 1991). In T2 solid, the Lu second and third shells consist in Fe and O atoms which can only be explained by a goethite-like structure. Furthermore, these shells are located at interatomic distances only slightly longer than  $d(\text{Fe—Fe}) = 3.02$  Å and  $d(\text{Fe—O}) = 3.22$  Å in goethite and can be explained by the difference in ionic radii (Shannon 1976) between <sup>VI</sup>Fe(III)

**Fig. 4** Lu  $L_3$  edge XANES (left panel), experimental (black line) and modeled (red line) EXAFS spectra (middle panel), and the corresponding Fourier transforms (right panel) of the samples and reference compounds. Fit results are given in Table 2



(0.65  $\text{\AA}$ ) and  $^{VI}\text{Lu(III)}$  (0.86  $\text{\AA}$ ). Also, the Fe2 shell in T2 solid would be compatible with the next nearest Fe shell in goethite. Finally, Lu incorporation into hematite can also be dismissed because the chemical environment of Lu in T2 solid differs from that reported for Lu-containing hematite (Dardenne et al. 2002).

## Discussion

Ferrihydrite is thermodynamically unstable and with time transforms into goethite, hematite, or a mixture of both (Schwertmann and Cornell 1991). The nature of the predominant transformation mechanism depends primarily on suspension pH (Cornell et al. 1989; Schwertmann and Murad 1983), and hematite and goethite are formed through competitive reactions. Maximum hematite formation is expected between pH 7 and 8, and maximum goethite formation at pH around 4 and 12. In this study, the suspension pH (5.67(5)) was intermediate between that leading to maximum formation of hematite and that leading to maximum formation of goethite, and thus favorable to the simultaneous formation of both phases. Assuming in first approximation that hematite formed (internal dehydration/rearrangement within Fh particles) faster than goethite (Fh dissolution followed by goethite nucleation), it may have served as substrate for the growth of goethite resulting in a structural association of both phases. The very similar solubility products (Chivot 2004) of hematite ( $K_s = 10^{-42.0}$ ) and goethite ( $K_s = 10^{-42.3}$ ) rule out the hypothesis of a dissolution/crystallization mechanism transforming one phase into the other. In addition, goethite possibly also

nucleated in solution but certainly in lower amounts than that grown on hematite.

Other parameters such as initial  $\text{Fe(III)}_{\text{aq}}$  concentration and rate of hydrolysis (Schwertmann and Cornell 1991) can affect the Fh transformation pathway. Generally, the presence of additives adsorbing at the surface of ferrihydrite or structurally incorporated foreign cations can interfere (e.g., stabilize against internal rearrangement and against dissolution) with the transformation (Cornell et al. 1987; Cornell et al. 1989; Freyria et al. 2013). In solution, complexing agents of Fe ions can hinder nucleation and growth of goethite. Significant amounts of Lu(III) were added ( $[\text{Lu(III)}]_{\text{tot}} = 1.6 \times 10^{-4}$  mol/L) to the starting Fh suspension, and Lu(III) forms bidentate complexes at the surface of Fh (Dardenne et al. 2001). Considering a mass concentration of 2.7 g/L Fh and a surface site density of  $1.71 \times 10^3$  mol/g (Dardenne et al. 2001), the surface coverage was  $< 10\%$  considering quantitative adsorption. Though Lu(III) forms stable surface complexes, this surface coverage was certainly too low to hinder Fh transformation. Another important parameter governing Fh transformation is temperature: increasing temperature promotes Fh dehydration and agglomeration thereby favoring the transformation into hematite (Cornell et al. 1989; Schwertmann and Cornell 1991).

EXAFS spectroscopy is an element-sensitive technique probing all Lu species present in the sample (incorporated, surface retained, and/or dissolved) whatever the size or shape of particles present in the suspension, whereas AsFIFFF data are only representative of the recovered fraction. In sample T2 super, AsFIFFF indicates the presence of Fe particles

and homogeneous association of Lu with these particles but the recoveries are very low (~12% for Fe and <1% for Lu) and thus results cannot be considered representative of the whole sample. EXAFS data suggest that the supernatant contains predominantly dissolved Lu species, no significant fraction of structurally incorporated or surface bound Lu could be evidenced. The data obtained from both techniques strongly point to the largest portion of Lu in T2 super being present as dissolved species while only a minor fraction is homogeneously, and thus certainly structurally, associated with Fe phases. Furthermore, because only the presence of goethite NPs could be evidenced by SEM, the fraction of incorporated Lu can only be located within goethite, substituting for structural Fe(III). Since goethite formed by Fh dissolution and subsequent nucleation, Lu(III) can only have been taken up structurally during nucleation and/or growth. The Fe/Lu mass ratio determined by AsFIFFF/ICP-MS (i.e.,  $215 \pm 59$ ) fits also very well with the value of  $236 \pm 20$  reported recently (Bouby et al. *In Preparation*). In the starting sample, the retention of Lu at the surface of Fh was nearly quantitative (Dardenne et al. 2001). The fraction of surface retained Lu decreased upon aging and can originate either from a decrease in available surface area (lower for hematite and goethite than for ferrihydrite) and/or in differences in surface reactivity between Fh and the transformation products.

AsFIFFF data hinted at a structural Lu association with iron phases (hematite and/or goethite) in sample T2. EXAFS spectroscopy on T2 solid corroborated this finding and the detection of higher distances neighboring shells allowed identifying the host phase as being most likely goethite. The Fe/Lu mass ratio in the recovered fraction of T2 equals  $196 \pm 17$ , matching within uncertainties the value found by direct analysis of the solid (i.e.,  $186 \pm 6$ ). Since these ratios are very close to that reported for the Lu associated with goethite in sample T2 super, they strongly point to a preferential Lu incorporation into goethite overgrown on hematite particles present in sample T2.

In goethite, Fe is bound to hydroxyl groups (i.e.,  $\text{FeO}_3(\text{OH})_3$  octahedra), and in hematite, the arrangement of cations produces pairs of  $\text{FeO}_6$  octahedra, and each octahedron shares three edges and one face with neighboring octahedra (Cornell and Schwertmann 1996). The Fe environment is thus more constrained in  $\alpha\text{-Fe}_2\text{O}_3$  than in  $\alpha\text{-FeOOH}$ . Also, in order to fit structural sites within hematite or goethite Lu(III) has to lose coordinated hydration water molecules. The difference in size (Shannon 1976) between Lu(III) ( $r^{\text{VI}}\text{Lu(III)} = 0.86 \text{ \AA}$ ) and Fe(III) ( $r^{\text{VI}}\text{Fe(III)} = 0.65 \text{ \AA}$ ) is not negligible, rendering homovalent substitution at the same structural site during nucleation unlikely. In contrast, adsorption at the solid/liquid interface followed by overgrowth appears more likely to result in structural incorporation. Such mechanism has been shown to operate for systems where the incorporated and the substituted species are of different charge

(e.g., (Schmidt et al. 2008)) and slightly different geometry (e.g., (Heberling et al. 2014)). Recent investigations indicated a similar metal ion uptake mechanism by iron oxyhydroxides at temperatures ranging from ~20 to 75 °C (e.g., Cu (Stegemeier et al. 2015)). Initially retained by the pre-formed solid, a fraction of surface sorbed ions was desorbed and with increasing contact time it was taken up structurally during particle growth by oriented aggregation. In any case kinetics of growth and degree of solid phase oversaturation may play key roles. Additionally, an incorporation following this pathway would result in Lu(III) homogeneously distributed within the goethite lattice as a consequence of enrichment upon goethite growth and not located at specific sites such as, e.g., close to the surface forming a rim or accumulated at the center of the particle resulting from incorporation upon nucleation. Furthermore, this growth mechanism is a dynamical process at the solid/liquid interface with exchange of species between the growing goethite and the contacting fluid. Consequently, if Lu(III) is still present at octahedral Fe(III) sites within goethite then the incorporated species must be stable; otherwise, it would have been released upon exchange between the solid phase and the contacting fluid. Following its release from the bulk solid, Lu(III) would adsorb at the surface of the solid. The absence of detected surface adsorbed Lu(III) species further supports Lu incorporation within the solid phase. This hypothesis (i.e., a preferential Lu incorporation into the overgrown goethite) and the absence of significant amounts of Lu(III) incorporated within hematite has been very successfully proved by TEM analysis and corroborated by DFT calculations in an companion paper (Yokosawa et al. 2018).

At elevated temperatures, hydration water molecules bound to Lu(III) may be more labile than at room temperature and Fh aggregation and dehydration promote the formation of hematite. Both reactions collectively favored Lu(III) incorporation within hematite upon tempering Fh in the presence of Lu(III) for 10 days at 70 °C (Dardenne et al. 2002; Bouby et al. 2004). Accordingly, only negligible amounts of Lu may be incorporated within goethite under these conditions. At room temperature, goethite formation proceeded via Fh dissolution followed by nucleation and growth (Schwertmann and Cornell 1991). Results from this study point to Lu(III) incorporation within goethite upon Fh aging at room temperature where hydration water molecules may be retained slightly more tightly, thereby preventing incorporation within the compact hematite structure. Note that Fe in goethite is bound to three hydroxyl groups in contrast to Fe within hematite. Proton exchange between coordinated and bulk water molecules may result in Lu ligated to -OH groups (i.e.,  $\text{Lu}(\text{H}_2\text{O})_{8-x}(\text{OH})_x$ ) which can be considered in first approximation similar to Fe bound to -OH in goethite, implying that Lu substitution for Fe within goethite may be possible.

In their investigations, Bouby et al. (*In Preparation*) used a sample obtained by aging for 15 years at room temperature the same sample which was initially tempered for 10 days at 70 °C (Dardenne et al. 2002; Bouby et al. 2004). In the tempered sample, Lu was found preferentially incorporated within hematite. After an additional 15 years aging time at room temperature, the sample still contained hematite and goethite, and, interestingly, the analysis indicated that besides Lu structurally incorporated within hematite, a portion of the lanthanide was also found structurally incorporated within goethite. In the present study, the transformation of Fh in the presence of Lu(III) but without initially tempering at 70 °C results in an incorporation only within goethite. Both studies are consistent with Lu(III) substituting for Fe(III) within goethite upon nucleation and growth at room temperature.

## Conclusion

Ferrihydrite was aged in the presence of Lu(III) for 12 years under ambient conditions at close to circumneutral conditions. Hematite and goethite formed as transformation products and Lu(III) was partitioned between the solid Fe phases and the liquid phase after aging. After centrifugation, the settled particles consist of hematite with overgrown goethite, whereas the supernatant contains only nanoparticulate goethite. Information on the Lu(III) binding mode was obtained by combining AsFIFFF and EXAFS spectroscopy. In the supernatant, the largest fraction of Lu(III) is present as dissolved species and a minor fraction is homogeneously associated with goethite, certainly structurally incorporated within this solid substituting randomly for octahedral Fe(III). In the settled particles, Lu(III) is homogeneously (no neighboring Lu atom was detected by EXAFS spectroscopy) and thus structurally associated with a solid phase. The sixfold coordination by oxygen atoms can only be explained by structural incorporation whereby Lu(III) substitutes for octahedral Fe(III). The nature of backscatters surrounding Lu(III) beyond the first shell can only be explained by a goethite-like structure. The presence of a Lu-containing hematite species was ruled out and no surface adsorbed Lu(III) could be evidenced.

Compared to earlier transformation experiments performed at elevated temperature, this study provides significant evidence on the influence of temperature on the fate of Lu(III) during ferrihydrite transformation when Lu was added after ferrihydrite precipitation. At room temperature, Lu incorporation within goethite (individual needles or overgrown on hematite) is observed and not within hematite. Recent findings indicate a preferential Lu incorporation within hematite upon aging in the presence of Lu(III) pre-formed ferrihydrite at elevated temperatures for several days, and after additional 15 years aging at room temperature, Lu(III) is found distributed into both hematite and goethite (Bouby et al. *In*

*Preparation*). In conclusion, without tempering it is very likely that the trivalent actinides may only be structurally retained within goethite. Another major outcome is the stability of the incorporated species. Data indicate that Lu(III) might be scavenged efficiently at least during 12 years under defined laboratory conditions. Further studies would be needed to investigate on the stability of these NPs under real conditions, i.e., in the presence of complexing ligands. Such information would greatly help improving our understanding on NPs mobility and provide valuable input for safety performance assessment of deep nuclear waste disposal sites.

**Acknowledgements** We thank S. Heck (KIT INE) for ICP OES, F. Geyer (KIT INE) for ICP MS analyses, and E. Soballa (KIT INE) for SEM measurements. We acknowledge the synchrotron light source ANKA (Karlsruhe, Germany) for the provision of synchrotron radiation beamtime.

## References

- Ankudinov AL, Ravel B, Rehr JJ, Conradson SD (1998) Real space multiple scattering calculations and interpretation of x ray absorption near edge structure. *Phys Rev B* 58(12):7565–7576. <https://doi.org/10.1103/PhysRevB.58.7565>
- Bianconi A, Dell’Ariccia M, Gargano A, Natoli CR (1983) Bond length determination using XANES. In: Bianconi A, Incoccia L, Stipcich S (eds) EXAFS and near edge structure. Springer Verlag, Berlin, pp 57–61. [https://doi.org/10.1007/978-3-642-50098-5\\_8](https://doi.org/10.1007/978-3-642-50098-5_8)
- Bots P, Shaw S, Law GTW, Marshall TA, Mosselmans JFW, Morris K (2016) Controls on the fate and speciation of Np(V) during iron (oxyhydr)oxide crystallization. *Environ Sci Technol* 50(7):3382–3390. <https://doi.org/10.1021/acs.est.5b05571>
- Bouby M, Geckeis H, Manh TN, Yun JI, Dardenne K, Schafer T, Walther C, Kim JI (2004) Laser induced breakdown detection combined with asymmetrical flow field flow fractionation: application to iron oxo/hydroxide colloid characterization. *J Chromatogr A* 1040(1):97–104. <https://doi.org/10.1016/j.chroma.2004.03.047>
- Bouby M, Geckeis H, Geyer FW (2008) Application of asymmetric flow field flow fractionation (AsFIFFF) coupled to inductively coupled plasma mass spectrometry (ICPMS) to the quantitative characterization of natural colloids and synthetic nanoparticles. *Anal Bioanal Chem* 392(7–8):1447–1457. <https://doi.org/10.1007/s00216-008-2422-0>
- Bouby M, Geckeis H, Lutzenkirchen J, Mihai S, Schäfer T (2011) Interaction of bentonite colloids with Cs, Eu, Th and U in presence of humic acid: a flow field flow fractionation study. *Geochim Cosmochim Acta* 75(13):3866–3880. <https://doi.org/10.1016/j.gca.2011.04.015>
- Bouby M, Finck N, Geckeis H (2012) Flow field flow fractionation (FIFFF) coupled to sensitive detection techniques: a way to examine radionuclide interactions with nanoparticles. *Mineral Mag* 76(7):2709–2721. <https://doi.org/10.1180/minmag.2012.076.7.06>
- Bouby M, Finck N, Geckeis H (2015) Synthetic smectites colloids: characterization of nanoparticles after co precipitation in the presence of lanthanides and tetravalent elements (Zr, Th). *Chromatography* 2(3):545–566. <https://doi.org/10.3390/chromatography2030545>
- Boudeulle M, Muller JP (1988) Structural characteristics of hematite and goethite and their relationships with kaolinite in a laterite from Cameroon—a TEM study. *Bull Mineral* 111:149–166

- Carlson L, Schwertmann U (1981) Natural ferrihydrites in surface deposits from Finland and their association with silica. *Geochim Cosmochim Acta* 45(3):421–429. [https://doi.org/10.1016/0016-7037\(81\)90250-7](https://doi.org/10.1016/0016-7037(81)90250-7)
- Chivot J (2004) Thermodynamique des produits de corrosion : Fonctions thermodynamiques, diagrammes de solubilité, diagrammes E-pH des systèmes Fe-H<sub>2</sub>O, Fe-CO<sub>2</sub>-H<sub>2</sub>O, Fe-S-H<sub>2</sub>O, Cr-H<sub>2</sub>O et Ni-H<sub>2</sub>O en fonction de la température. ANDRA, Châtenay-Malabry
- Cornell RM (1985) Effect of simple sugars on the alkaline transformation of ferrihydrite into goethite and hematite. *Clays Clay Min* 33(3):219–227. <https://doi.org/10.1346/CCMN.1985.0330308>
- Cornell RM, Schwertmann U (1996) The iron oxides: structure, properties, reactions, occurrences and uses. VCH, Weinheim
- Cornell RM, Giovanoli R, Schindler PW (1987) Effect of silicate species on the transformation of ferrihydrite into goethite and hematite in alkaline media. *Clays Clay Min* 35(1):21–28. <https://doi.org/10.1346/CCMN.1987.0350103>
- Cornell RM, Giovanoli R, Schneider W (1989) Review of the hydrolysis of iron(III) and the crystallization of amorphous iron(III) hydroxide hydrate. *J Chem Technol Biotechnol* 46:115–134
- Cornell RM, Schneider W, Giovanoli R (1992) The effect of nickel on the conversion of amorphous iron(III) hydroxide into more crystalline iron oxides in alkaline media. *J Chem Technol Biotechnol* 53:73–79
- Cudennec Y, Lecerf A (2006) The transformation of ferrihydrite into goethite and hematite, revised. *J Solid State Chem* 179(3):716–722. <https://doi.org/10.1016/j.jssc.2005.11.030>
- Dardenne K, Schafer T, Denecke MA, Rothe J, Kim JI (2001) Identification and characterization of sorbed lutetium on 2-line ferrihydrite by sorption data modeling. *TRLS EXAFS Radiochim Acta* 89(7):469–479. <https://doi.org/10.1524/ract.2001.89.7.469>
- Dardenne K, Schafer T, Lindqvist Reis P, Denecke MA, Plaschke M, Rothe J, Kim JI (2002) Low temperature XAFS investigations on the lutetium binding changes during the 2-line ferrihydrite alteration process. *Environ Sci Technol* 36(23):5092–5099. <https://doi.org/10.1021/es025513f>
- Finck N, Schlegel ML, Bosbach D (2009) Sites of Lu(III) sorbed to and coprecipitated with hectorite. *Environ Sci Technol* 43(23):8807–8812. <https://doi.org/10.1021/es901940v>
- Finck N, Bouby M, Dardenne K, Geckeis H (2012) Characterization of Eu(III) coprecipitated with and adsorbed on hectorite: from macroscopic crystallites to nanoparticles. *Mineral Mag* 76(7):2723–2740. <https://doi.org/10.1180/minmag.2012.076.7.07>
- Finck N, Nedel S, Dideriksen K, Schlegel ML (2016) Trivalent actinide uptake by iron (hydr)oxides. *Environ Sci Technol* 50(19):10428–10436. <https://doi.org/10.1021/acs.est.6b02599>
- Ford RG, Bertsch PM, Farley KJ (1997) Changes in transition and heavy metal partitioning during hydrous iron oxide aging. *Environ Sci Technol* 31(7):2028–2033. <https://doi.org/10.1021/es960824a>
- Freyria FS, Barrera G, Tiberto P, Belluso E, Levy D, Saracco G, Allia P, Garrone E, Bonelli B (2013) Eu-doped alpha-Fe<sub>2</sub>O<sub>3</sub> nanoparticles with modified magnetic properties. *J Solid State Chem* 201:302–311. <https://doi.org/10.1016/j.jssc.2013.03.018>
- Giddings JC (1993) Field flow fractionation: analysis of macromolecular, colloidal, and particulate materials. *Science* 260(5113):1456–1465. <https://doi.org/10.1126/science.8502990>
- Giddings JC, Yang FJ, Myers MN (1976) Theoretical and experimental characterization of flow field flow fractionation. *Anal Chem* 48(8):1126–1132. <https://doi.org/10.1021/ac50002a016>
- Hazemann JL, Berar JF, Manceau A (1991) Rietveld studies of the aluminium-iron substitution in synthetic goethite. *Mater Sci Forum* 79:821–826. <https://doi.org/10.4028/www.scientific.net/MSF.79.82.821>
- Heberling F, Vinograd VL, Polly R, Gale JD, Heck S, Rothe J, Bosbach D, Geckeis H, Winkler B (2014) A thermodynamic adsorption/entrapment model for selenium(IV) coprecipitation with calcite. *Geochim Cosmochim Acta* 134:16–38. <https://doi.org/10.1016/j.gca.2014.02.044>
- Hiemstra T, Van Riemsdijk WH (2009) A surface structural model for ferrihydrite I: sites related to primary charge, molar mass, and mass density. *Geochim Cosmochim Acta* 73(15):4423–4436. <https://doi.org/10.1016/j.gca.2009.04.032>
- Huber F, Enzmann F, Wenka A, Bouby M, Dentz M, Schafer T (2012) Natural micro-scale heterogeneity induced solute and nanoparticle retardation in fractured crystalline rock. *J Contam Hydrol* 133:40–52. <https://doi.org/10.1016/j.jconhyd.2012.03.004>
- Jambor JL, Dutrizac JE (1998) Occurrence and constitution of natural and synthetic ferrihydrite, a widespread iron oxyhydroxide. *Chem Rev* 98(7):2549–2586. <https://doi.org/10.1021/cr970105t>
- Lion LW, Altmann RS, Leckie JO (1982) Trace metal adsorption characteristics of estuarine particulate matter: evaluation of contributions of iron/manganese oxide and organic surface coatings. *Environ Sci Technol* 16(10):660–666. <https://doi.org/10.1021/es00104a007>
- Lu N, Kung KS, Mason CFV, Triay IR, Cotter CR, Pappas AJ, Pappas MEG (1998) Removal of plutonium-239 and americium-241 from Rocky Flats soils by leaching. *Environ Sci Technol* 32(3):370–374. <https://doi.org/10.1021/es970329t>
- Marshall TA, Morris K, Law GTW, Livens FR, Mosselmans JFW, Bots P, Shaw S (2014) Incorporation of uranium into hematite during crystallization from ferrihydrite. *Environ Sci Technol* 48(7):3724–3731. <https://doi.org/10.1021/es500212a>
- Maslen EN, Streltsov VA, Streltsova NR, Ishizawa N (1994) Synchrotron X-ray study of the electron density in  $\alpha$ -Fe<sub>2</sub>O<sub>3</sub>. *Acta Crystallogr B* 50(4):435–441. <https://doi.org/10.1107/S0108768194002284>
- Nagano T, Mitamura H, Nakayama S, Nakashima S (1999) Formation of goethite and hematite from neodymium-containing ferrihydrite suspensions. *Clays Clay Min* 47(6):748–754. <https://doi.org/10.1346/CCMN.1999.0470609>
- Ngo Manh T, Geckeis H, Kim JI, Beck HP (2001) Application of the flow field flow fractionation (FFFF) to the characterization of aquatic humic colloids: evaluation and optimization of the method. *Colloids Surf A Physicochem Eng Asp* 181(1–3):289–301. [https://doi.org/10.1016/S0927-7757\(00\)00803-7](https://doi.org/10.1016/S0927-7757(00)00803-7)
- Novikov AP, Kalmykov SN, Utsunomiya S, Ewing RC, Horreard F, Merkulov A, Clark SB, Tkachev YY, Myasoedov BF (2006) Colloid transport of plutonium in the far field of the Mayak production association, Russia. *Science* 314(5799):638–641. <https://doi.org/10.1126/science.1131307>
- Ohta A, Kagi H, Nomura M, Tsuno H, Kawabe I (2009) Coordination study of rare earth elements on Fe oxyhydroxide and Mn dioxides: part II. Correspondence of structural change to irregular variations of partitioning coefficients and tetrad effect variations appearing in interatomic distances. *Am Mineral* 94(4):476–486. <https://doi.org/10.2138/am.2009.2987>
- Persson I, D'Angelo P, De Panfilis S, Sandstrom M, Eriksson L (2008) Hydration of lanthanoid(III) ions in aqueous solution and crystalline hydrates studied by EXAFS spectroscopy and crystallography: the myth of the « gadolinium break ». *Chem Eur J* 14(10):3056–3066. <https://doi.org/10.1002/chem.200701281>
- Phelan FR Jr, Bauer BJ (2007) Simulation of nanotube separation in field flow fractionation (FFF). *Chem Eng Sci* 62(17):4620–4635. <https://doi.org/10.1016/j.ces.2007.04.019>
- Phelan FR Jr, Bauer BJ (2009) Comparison of steric effects in the modeling of sphere and rodlike particles in field flow fractionation. *Chem Eng Sci* 64(8):1747–1758. <https://doi.org/10.1016/j.ces.2008.10.006>
- Qi Z, Liu M, Chen Y, Zhang G, Xu M, Shi C, Zhang W, Yin M, Xie Y (2007) Local structure of nanocrystalline Lu<sub>2</sub>O<sub>3</sub>:Eu studied by X-ray absorption spectroscopy. *J Phys Chem C* 111(5):1945–1950. <https://doi.org/10.1021/jp066937p>
- Ravel B, Newville M (2005) ATHENA, ARTEMIS, HEPHAESTUS: data analysis for X-ray absorption spectroscopy using *IFEFFIT*. *J*

- Synchrotron Radiat 12(4):537–541. <https://doi.org/10.1107/S0909049505012719>
- Rothe J, Butorin S, Dardenne K, Denecke MA, Kienzler B, Loble M, Metz V, Seibert A, Steppert M, Vitova T, Walther C, Geckeis H (2012) The INE beamline for actinide science at ANKA. *Rev Sci Instrum* 83(4):043105. <https://doi.org/10.1063/1.3700813>
- Schäfer T, Artinger R, Dardenne K, Bauer A, Schuessler W, Kim JI (2003) Colloid borne americium migration in Gorleben groundwater: significance of iron secondary phase transformation. *Environ Sci Technol* 37(8):1528–1534. <https://doi.org/10.1021/es015832r>
- Schimpf ME, Caldwell K, Giddings JC (2000) *Field flow fractionation handbook*. Wiley Interscience, John Wiley & Sons, New York ISBN: 978 0471184300
- Schmidt M, Stumpf T, Marques Fernandes M, Walther C, Fanghänel T (2008) Charge compensation in solid solutions. *Angew Chem Int Ed* 47(31):5846–5850. <https://doi.org/10.1002/anie.200705827>
- Schwertmann U, Cornell RM (1991) Iron oxides in the laboratory. Preparation and characterization. VCH, Weinheim
- Schwertmann U, Murad E (1983) Effect of pH on the formation of goethite and hematite from ferrihydrite. *Clays Clay Min* 31(4):277–284. <https://doi.org/10.1346/CCMN.1983.0310405>
- Shannon RD (1976) Revised effective ionic radii and systematic studies of interatomic distances in halides and chalcogenides. *Acta Crystallogr Sect A* 32(5):751–767. <https://doi.org/10.1107/S0567739476001551>
- Sharma V, Park K, Srinivasarao M (2009) Shape separation of gold nanorods using centrifugation. *Proc Natl Acad Sci* 106(13):4981–4985. <https://doi.org/10.1073/pnas.0800599106>
- Stegemeier JP, Reinsch BC, Lentini CJ, Dale JG, Kim CS (2015) Aggregation of nanoscale iron oxyhydroxides and corresponding effect on metal uptake, retention, and speciation: II. Temperature and time. *Geochim Cosmochim Acta* 148:113–129. <https://doi.org/10.1016/j.gca.2014.08.031>
- Stumpf S, Stumpf S, Dardenne K, Hennig C, Foerstendorf H, Klenze R, Fanghänel T (2006) Sorption of Am(III) onto 6 line ferrihydrite and its alteration products: investigations by EXAFS. *Environ Sci Technol* 40(11):3522–3528. <https://doi.org/10.1021/es052518e>
- Sun T, Paige CR, Snodgrass WJ (1996) The effect of cadmium on the transformation of ferrihydrite into crystalline products at pH 8. *Water Air Soil Pollut* 91(3–4):307–325. <https://doi.org/10.1007/BF00666266>
- Wahlund KG, Giddings JC (1987) Properties of an asymmetrical flow field flow fractionation channel having one permeable wall. *Anal Chem* 59(9):1332–1339. <https://doi.org/10.1021/ac00136a016>
- Wijnhoven JEGJ, Koorn JP, Poppe H, Kok WT (1996) Influence of injected mass and ionic strength on retention of water soluble polymers and proteins in hollow fibre flow field flow fractionation. *J Chromatogr A* 732(2):307–315. [https://doi.org/10.1016/0021-9673\(95\)01263-X](https://doi.org/10.1016/0021-9673(95)01263-X)
- Yokosawa T, Prestat E, Polly R, Bouby M, Dardenne K, Finck N, Haigh SJ, Denecke MA, Geckeis H (2018) Fate of Lu(III) sorbed on 2 line ferrihydrite at pH 5.7 and aged for 12 years at room temperature. II: insights from STEM EDXS and DFT calculations. *Environ Sci Pollut Res (In this issue)*

## Repository KITopen

Dies ist ein Postprint/begutachtetes Manuskript.

Empfohlene Zitierung:

Finck, N.; Bouby, M.; Dardenne, K.

[Fate of Lu\(III\) sorbed on 2-line ferrihydrite at pH 5.7 and aged for 12 years at room temperature. I: insights from ICP-OES, XRD, ESEM, AsFIFFF/ICP-MS, and EXAFS spectroscopy](#)

2019. Environmental science and pollution research, 26

[doi: 10.554/IR/1000089569](#)

Zitierung der Originalveröffentlichung:

Finck, N.; Bouby, M.; Dardenne, K.

[Fate of Lu\(III\) sorbed on 2-line ferrihydrite at pH 5.7 and aged for 12 years at room temperature. I: insights from ICP-OES, XRD, ESEM, AsFIFFF/ICP-MS, and EXAFS spectroscopy](#)

2019. Environmental science and pollution research, 26 (6), 5238–5250.

[doi:10.1007/s11356-018-1314-x](#)

Lizenzinformationen: [KITopen-Lizenz](#)